PNAS RESEARCH ARTICLE | PHYSIOLOGY

Intraluminal pressure elevates intracellular calcium and contracts CNS pericytes: Role of voltage-dependent calcium channels

Nicholas R. Klug[a,1], Maria Sancho[a], Albert L. Gonzales[a,b], Thomas J. Heppner[a], Rochelle Irene C. O'Brien[a], David Hill-Eubanks[a], and Mark T. Nelson[a,c,1]

Contributed by Mark T. Nelson; received September 27, 2022; accepted January 24, 2023; reviewed by Jessica Filosa and Madeline Nieves-Cintrón

Arteriolar smooth muscle cells (SMCs) and capillary pericytes dynamically regulate blood flow in the central nervous system in the face of fluctuating perfusion pressures. Pressure-induced depolarization and Ca^{2+} elevation provide a mechanism for regulation of SMC contraction, but whether pericytes participate in pressure-induced changes in blood flow remains unknown. Here, utilizing a pressurized whole-retina preparation, we found that increases in intraluminal pressure in the physiological range induce contraction of both dynamically contractile pericytes in the arteriole-proximate transition zone and distal pericytes of the capillary bed. We found that the contractile response to pressure elevation was slower in distal pericytes than in transition zone pericytes and arteriolar SMCs. Pressure-evoked elevation of cytosolic Ca^{2+} and contractile responses in SMCs were dependent on voltage-dependent Ca^{2+} channel (VDCC) activity. In contrast, Ca^{2+} elevation and contractile responses were partially dependent on VDCC activity in transition zone pericytes and independent of VDCC activity in distal pericytes. In both transition zone and distal pericytes, membrane potential at low inlet pressure (20 mmHg) was approximately −40 mV and was depolarized to approximately −30 mV by an increase in pressure to 80 mmHg. The magnitude of whole-cell VDCC currents in freshly isolated pericytes was approximately half that measured in isolated SMCs. Collectively, these results indicate a loss of VDCC involvement in pressure-induced constriction along the arteriole-capillary continuum. They further suggest that alternative mechanisms and kinetics of Ca^{2+} elevation, contractility, and blood flow regulation exist in central nervous system capillary networks, distinguishing them from neighboring arterioles.

pericytes | vascular tone | cerebral blood flow | autoregulation

Significance

Capillaries account for ~90% of all blood vessels in the central nervous system, allowing for robust nutrient and waste exchange. Capillary endothelial cells are variably covered with pericytes, which contract and dilate on slow or rapid timescales depending on their proximity to upstream arterioles. The resulting regulation of capillary blood flow is critical for brain health, but physiological stimuli that regulate this process are unclear. Here, using a pressurized retinal vascular preparation, we demonstrate that intraluminal pressure is an intrinsic stimulus for pericyte calcium elevation and constriction in proximal and distal capillary branches. Moreover, the involvement of voltage-dependent calcium channels decreases with distance from the upstream arteriole, highlighting differences in contractile properties between pericytes and neighboring arteriolar smooth muscle cells.

The ever-changing metabolic needs of neurons and glia in the central nervous system (CNS) are continuously met by moment-to-moment regulation of arteriole-mediated blood flow, a regulatory property that further serves to protect the microvasculature from high perfusion pressures. In cerebral arteries and arterioles, increases in intravascular pressure cause membrane depolarization, activation of voltage-dependent Ca^{2+} channels (VDCCs), elevation of intracellular Ca^{2+} and contraction of smooth muscle cells (SMCs), a mechanism intrinsic to SMCs termed the "myogenic response" (1, 2). To put this in a quantitative context, we previously reported that an increase in intraluminal pressure from a low value (5 mmHg) to a physiological value (40 mmHg) depolarizes SMCs in brain parenchymal arterioles from −58 mV to −35 mV, resulting in elevation of cytosolic Ca^{2+} from 120 nM to 260 nM, an effect that is blocked by VDCC inhibitors (2). This pressure-sensitive autoregulatory process not only enables maintenance of constant blood delivery in the CNS during rapid (postural change) or sustained (diurnal blood pressure patterns, exercise) alterations in perfusion pressure (3), it is also critical for creating the basal level of vascular constriction (i.e., tone) required for neuronal activity-dependent dilation and increased blood flow ("functional hyperemia") mediated by neurovascular coupling mechanisms.

In the CNS vasculature, including the brain and retinal circulation, as elsewhere in the body, terminal arterioles give way to networks of capillaries that are covered by perivascular cells. These cells, termed pericytes, exhibit graded changes in morphology and physiological properties as a function of distance from the terminal arteriole and have been shown to direct blood flow within the capillary network (4–9). Capillary segments in the postarteriole transition zone, corresponding to the first approximately three to four capillary branches, are encased by dynamically contractile pericytes that are capable of rapidly contracting and relaxing to regulate downstream capillary blood flow (4–8, 10–12). These transition zone pericytes contain many of the same proteins involved in excitation–contraction coupling as SMCs, such as VDCCs (Cav1.2), alpha smooth muscle actin (αSMA), smooth muscle myosin heavy chain (SMMHC), and myosin light chain kinase (4, 13, 14). In contrast to these arteriole-proximate transition zone pericytes, which are

Author contributions: N.R.K. and M.T.N. designed research; N.R.K. developed experimental procedures; N.R.K., M.S., A.L.G., T.J.H., and R.I.C.O. performed research; N.R.K. and M.S. analyzed data; and N.R.K., D.H.-E., and M.T.N. wrote the paper.

Reviewers: J.F., Augusta University; and M.N.-C., University of California, Davis.

The authors declare no competing interest.

[1]To whom correspondence may be addressed. Email: nicholas.klug@uvm.edu or mark.nelson@uvm.edu.

This article contains supporting information online at https://www.pnas.org/lookup/suppl/doi:10.1073/pnas.2216421120/-/DCSupplemental.

Published February 21, 2023.

characterized by their ensheathing or mesh-type projections, capillary pericytes at more distal locations exhibit a thin-stranded morphology, lack detectable αSMA expression, and do not rapidly regulate blood flow. Instead, they exhibit a much slower form of capillary blood flow regulation (15, 16) that has mainly been implicated in reduced capillary flow during disease (8, 11, 17). However, whether changes in intralumenal pressure differentially affect membrane potential, cytosolic Ca^{2+}, and contractility in transition zone and distal pericytes, and how VDCCs functionally contribute to this process, are not known.

To explore these fundamental issues, we examined vascular responses to various perfusion pressures using an en face, intact retina preparation in which the retinal microvascular tree is pressurized by cannulating the ophthalmic artery (4, 18–20). Arteriole and capillary vessel diameters were assessed using an exogenous vessel-specific stain (fluorescent isolectin), and abluminal edges of the vessels and changes in intracellular Ca^{2+} levels were measured by monitoring SMC/pericyte GCaMP6f (genetically encoded Ca^{2+} indicator) fluorescence. Pericyte membrane potential was measured using dye-filled microelectrodes, and VDCC activity in freshly isolated SMCs and pericytes was determined using patch-clamp electrophysiology. We found that increases in intraluminal pressure resulted in Ca^{2+} elevation and sustained contraction of SMCs in arterioles and pericytes in both transition zone and distal capillaries, although pressure-induced constrictions were slower in transition zone pericytes than arteriolar SMCs and slower still in distal capillaries. We further found that pressure-induced Ca^{2+} elevation and constriction were dependent on VDCCs in arteriolar SMCs, partially dependent on VDCCs in transition zone pericytes, and independent of VDCCs in distal pericytes. Notably, inhibition of G_q-protein-coupled receptor (G_qPCR) signaling in the presence of the VDCC inhibitor nifedipine reduced pressure-induced cytosolic Ca^{2+} elevations, suggesting a role for G_qPCRs in the VDCC-independent component of transition zone/distal pericyte contraction. These differences in the VDCC-dependence of pressure-induced constriction and Ca^{2+} elevation between arteriolar SMCs and pericytes were associated with a fundamental difference in the membrane potential of SMCs (approximately −60 mV) and transition zone/distal pericytes (approximately −40 mV) at low baseline inlet pressure (20 mmHg), and approximately twofold larger VDCC currents in SMCs compared with transition zone/distal pericytes. These results also highlight differences in the mechanisms that regulate contractility in pericytes and SMCs and suggest that, even at relatively depolarized membrane potentials, VDCC channel activity gradually becomes insufficient to sustain Ca^{2+} elevation and contractile responses in capillary pericytes as they transition from ensheathing/mesh type (arteriole-proximate) to thin-strand type (distal).

Results

Defining Vessels along the Arteriole–Capillary Axis in the Retina. To establish criteria for defining CNS vascular segments, we exploited the stereotyped angioarchitecture of the retina. Specifically, we performed fixed whole-mount retina imaging and live-tissue imaging in our recently developed, en face retina preparation, in which the entire retinal microvasculature is pressurized by raising pressure at the cannulated ophthalmic artery. Staining with isolectin, which specifically binds carbohydrate residues found on the vasculature (21), illuminates the contours of the entire retinal vasculature (Fig. 1*A*). Vascular segments are covered by SMCs and pericytes that show distinct, graded morphologies (8, 9). These unique transitioning morphologies from the arteriole into the capillary network were illustrated by imaging Ca^{2+}-sensitive green fluorescent protein (GFP) fluorescence using *Myh11*-GCaMP6f (cre^{ERT2}-loxP) mice (also used for live Ca^{2+} imaging; *SI Appendix*, *Methods*), which express the GFP-based, genetically encoded Ca^{2+} indicator, GCaMP6f, in SMCs and pericytes (Fig. 1 *A*, *Middle* and *Right*).

The terminal reach of arterioles radiating off the central retinal artery (fed by the ophthalmic artery) was determined by staining fixed retina tissue for elastin—a major component of the internal elastic lamina (IEL) (4, 18, 22) that physically separates endothelial cells and overlaying SMCs in arterioles and arteries. This procedure clearly distinguishes elastin-positive arterioles from laterally branching, elastin-negative downstream capillaries (4, 22, 23), drawing a sharp boundary between larger diameter (~20 to 25 μm) radiating arterioles and narrower diameter (typically <10 μm) capillaries, as seen in fixed (Fig. 1*B*) and live (Fig. 1*C*) tissues. On average, the first approximately four branches (3.8 ± 0.3) in the capillary network contained pericytes that stained prominently for αSMA (Fig. 1*B*), consistent with their reported contractile properties (4, 8, 18, 24). Despite expressing αSMA, pericytes in arteriole-proximate capillary branches can readily be distinguished from SMCs on molecular, morphological, and functional grounds (4, 8, 18). Thus, we consider all mural cells within the capillary network, as defined above, to be pericytes and refer to αSMA-expressing pericytes cells within the arteriole-proximate region of the capillary network (first approximately four capillary branches) as dynamically contractile pericytes, most of which exhibit an ensheathing morphology. This arteriole-proximal contractile capillary region, with its characteristic pericyte morphology and αSMA gradient, is unique compared with arterioles and distal capillaries and is here called the transition zone. In brain and retina tissue, approximately fifth-order and greater capillary branches are covered by thin-strand pericytes that typically lack αSMA, referred to here as distal pericytes (15, 24). The distinct changes in IEL coverage and pericyte morphology as arterioles transition to capillaries are illustrated in Fig. 1*D*.

Arterioles and Transition Zone/Distal Capillaries Differentially Constrict to Inlet Perfusion Pressure. To assess effects of pressure in intact CNS arterioles and capillaries, we imaged lectin-stained, whole-mount, pressurized en face retina preparations using high-resolution spinning-disk confocal microscopy, as illustrated in Fig. 2*A*. The degree of pressure-induced constriction was determined at inlet pressures (measured at the ophthalmic artery) that bracket the physiological range (20, 40, 60, 80, and 100 mmHg), estimated to be approximately 80 mmHg, or ~80% of mean arterial pressure (25–27). We defined constriction at a given intraluminal pressure as the decrease in diameter in a bath solution containing physiological external Ca^{2+} (2 mM) relative to passive diameter in 0 mM external Ca^{2+}. The duration of each pressure step was 10 min, and the average abluminal diameter was determined by acquiring a serial z-stack image (*SI Appendix*, *Methods*) from the last 30-s of the 10-min pressure step. Passive diameters were obtained following subsequent exposure to physiological salt solution without extracellular Ca^{2+}.

Representative images of arterioles and capillaries (transition zone and distal) depict contractile response to changes in ophthalmic artery inlet pressure (20, 40, 60, and 80 mmHg for arterioles and transition zone capillaries; 20 and 80 mmHg for distal capillaries; Fig. 2*B*). Branch-specific constriction of arterioles up to eighth capillary branches at inlet pressures of 20, 40, 60, 80, and 100 mmHg are shown in Fig. 2*C*. Significant constriction was observed at inlet pressures of 60 mmHg in the arteriole and first to fifth capillary branches, and all measured vessels significantly constricted at inlet pressures of 80 and 100 mmHg (Fig. 2*C*). Arterioles and transition

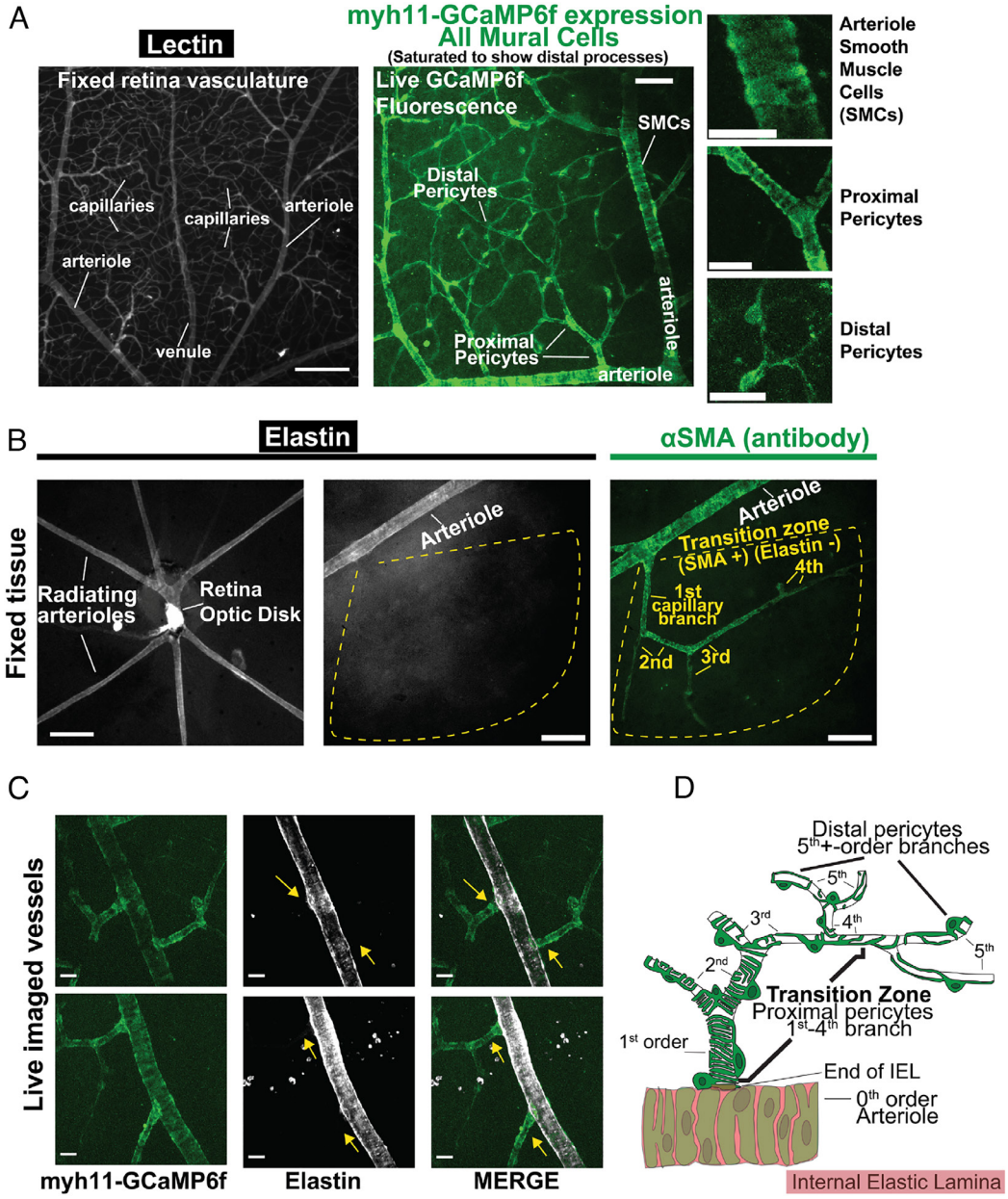

Fig. 1. Classification of vascular zones within the retinal vasculature. (*A*) *Left* panel, lectin staining of arterioles, capillaries, and venules. *Middle* panel, demonstration of fluorescence in *myh11*-GCaMP6f (SMMHC) vessels, showing SMCs (arterioles) and all pericytes (capillaries). *Right* panels, *Insets* from *Middle* panel showing mural cell morphology. [Scale bars, 200 μm (*Left* panel), 50 μm (*Middle* panel), and 20 μm (*Right Inset* panels).] (*B*) *Left* panel, low-magnification (10×, 0.1 Numerical Aperture) widefield image of radiating arterioles in a whole-mount retina preparation, visualized by staining for elastin (IEL). *Middle* and *Right* panels, 16× (0.8 Numerical Aperture) widefield image of radiating arteriole and proximal capillaries, visualized by staining for elastin (IEL, *Middle* panel) or αSMA (*Right* panel). Dotted yellow outline highlighting abrupt loss of elastin (IEL) and continued expression of αSMA in arteriole-proximate capillary branches; first, second, third, and fourth denote capillary branch order. On average, capillaries (vessels lacking an IEL) exhibited αSMA expression (fluorescence intensity > 2 SD above background) up to a branch order of 3.8 ± 0.3 (n = 31 arteriole-capillary segments from five mouse retinas). [Scale bars, 200 μm (*Left*) and 50 μm (*Middle* and *Right* panels).] (*C*) Representative images of live tissue showing the abrupt loss of the IEL at the point where lateral capillary branches begin (yellow arrows), demonstrated by GCaMP (GFP) fluorescence in vessels from *myh11*-GCaMP6f mice. (Scale bar, 20 μm.) (*D*) Schematic depiction of the transition zone comprising approximately the first four capillary segments, showing the banding of individual SMCs wrapping around arteriolar endothelial cells, the abrupt decrease in vessel diameter and loss of IEL at the beginning of the first-order capillary branch, and the transitioning morphology of overlying pericytes from enwrapping to mesh type to thin-strand with progression from first- to fifth- and higher order branches.

zone and distal capillaries exhibited graded constrictions in response to pressure, with arterioles being the most responsive (Fig. 2*D*). Baseline abluminal diameters (20 mmHg in [2 mM]$_{external}$ Ca^{2+}) for each vascular segment are shown in Fig. 2*E*. Although we used passive properties of vessels to accurately quantify constriction (Fig. 2*C*), we also evaluated absolute diameter changes in vessels (in μm) during pressure elevation in physiological 2 mM Ca^{2+} solution. Elevation of pressure produced significant reductions in diameters of transition zone and distal capillary vessels (Fig. 2*F*).

Flow Properties of the Pressurized Retina Preparation. Our data indicate that arterioles and capillaries in the pressurized retina preparation constrict to pressure in a graded manner, with a level of preconstriction allowing the diameter of arterioles to increase by ~7 μm and capillaries by 0.5 to 2.5 μm—values similar to those for functional dilations observed in vivo (5, 7, 28, 29). To determine whether these constrictions regulate flow, we visualized flow properties within this system by monitoring the flow of fluorescent beads (1 μm diameter, introduced into the

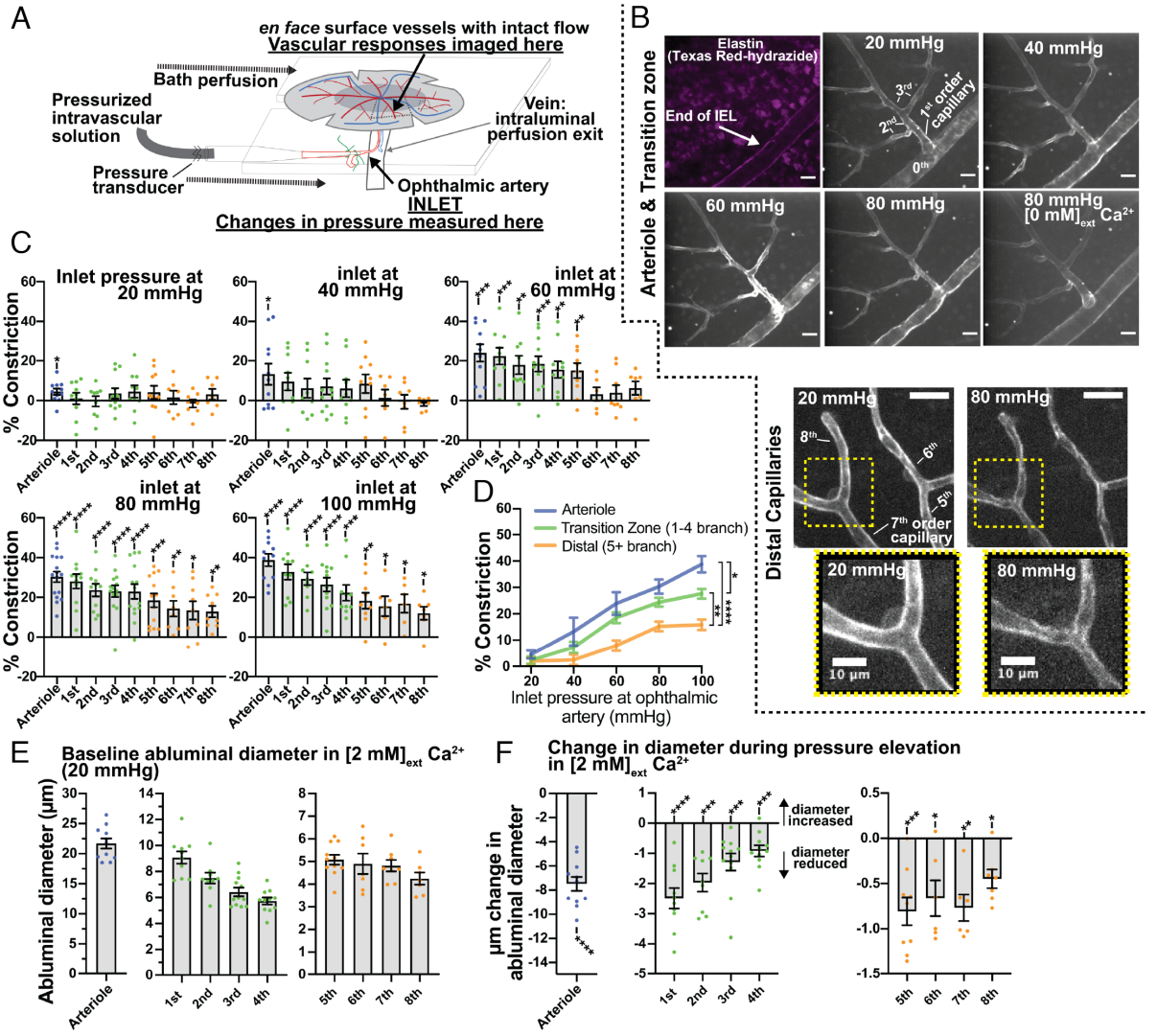

Fig. 2. Pressure-induced constriction in arterioles and capillaries. (*A*) Schematic depiction of the pressurized retina preparation. (*B*) *Top* panels: Z-projection of live lectin-stained arterioles and transition zone capillary branches at 20, 40, 60, and 80 mmHg, and 80 mmHg with 0 Ca^{2+}; each image was taken during the final minute of the pressure step. Texas Red hydrazide was added to stain the IEL and verify arteriole and capillary branch orders (first panel). *Bottom* panels: Z-projection of live lectin-stained distal capillary branches at 20 and 80 mmHg. (*C*) Percent vascular constriction in arterioles and first- to eighth-order capillary branches, measured at 20 to 100 mmHg in 2 mM external Ca^{2+} (active diameter) and 20 to 100 mmHg in 0 mM external Ca^{2+} with 5 mM ethylene glycol-bis (β-aminoethyl ether)-N,N,N′,N′-tetraacetic acid (EGTA) (passive diameter; *SI Appendix, Methods*). (*D*) Arteriole and transition zone and distal capillary pressure-constriction curves. (*E*) Baseline abluminal diameters of arterioles and first- to eighth-order capillary branches at a starting pressure of 20 mmHg. (*F*) Maximum changes in diameter observed in arterioles and first- to eighth-order capillary branches in [2 mM]ext Ca^{2+} during elevation of inlet pressure, ranging from 20 to 100 mmHg. Data are presented as individual values and mean ± SEM [n per branch = 6 to 12 from six animals; *C*, *F*: **P* < 0.05, ***P* < 0.01, ****P* < 0.001, *****P* < 0.0001 vs. theoretical mean of zero (no constriction), one sample *t* test, unmarked comparison are not significant; *D*: **P* < 0.05, ***P* < 0.01, ****P* < 0.001, *****P* < 0.0001, two-way ANOVA with Tukey's multiple comparison test at 100 mmHg]. (Scale bars, 20 µm unless otherwise labeled.)

cannula solution), which provide a readout of plasma flow, using widefield fluorescence microscopy (*SI Appendix*, Fig. S1*A*). Using this approach, it is possible to visualize both single-particle and whole-tissue flow patterns (*SI Appendix*, Fig. S1*B*).

The pressurized retina preparation is an intact-flow system, with perfusion starting at the ophthalmic artery and perfusate ultimately draining via the retinal vein. Under conditions in which the whole retina is imaged without fluorescently staining the vessels (i.e., fluorescent beads only) and at a zoom level sufficient to capture the entire preparation, the system resolution is such that diameters of relatively large retinal venules can be accurately discerned (*SI Appendix, Methods*). Because flow in venules is representative of cumulative upstream flow (i.e., through arterioles and capillaries) (30), we utilized venule flow as a readout for changes in flow rates through the whole intact retinal vasculature, assessing venule flow rates at different ophthalmic artery inlet pressures (20 to 100 mmHg). Flow rates increased at 40 mmHg and plateaued over the range of 60 to 100 mmHg (*SI Appendix*, Fig. S1*C*). At an inlet pressure of 80 mmHg, observed absolute plasma flow rates (0.63 to 1.89 µL/min) were in the range of in vivo measurements made in the mouse retina (31). Changes in network resistance, determined from flow rates and partial pressure differences (where the bath pressure at which beads drained was assumed to be 0 mmHg), increased sharply in the 80- to 100-mmHg range (*SI Appendix*, Fig. S1*D*). Application of a hyperpolarizing concentration of K^+ (10 mM), which activates Kir2 channels and dilates SMCs and transition zone pericytes (4), increased plasma flow rate, whereas addition of a depolarizing concentration of K^+ (30 mM), which activates VDCCs and constricts SMCs and transition zone pericytes, decreased flow rate (*SI Appendix*, Fig. S1*E*). These observations suggest that each vascular zone likely experiences physiological pressure and flow changes and that contractile responses are able to maintain relatively physiological outlet flow

values. These flow values can be manipulated by altering network resistances (vessel contractility) through hyperpolarization or depolarization of the vasculature.

Mechanisms of Sustained Constrictions in Arterioles and Transition Zone/Distal Capillaries. Pressure-induced constriction in cerebral arteries is dependent on VDCC activity in SMCs (1, 2). To determine the role of VDCCs in pressurized arterioles and capillaries, we measured dilatory responses to 500 nM nifedipine, a specific and potent VDCC inhibitor, in vessels 10 min after inducing a sustained constriction by elevating ophthalmic artery inlet pressure from 20 mmHg to 80 mmHg (Fig. 3*A*). As expected, nifedipine led to complete relaxation of arterioles, implying that Ca^{2+} influx through VDCCs is entirely responsible for sustained arteriole constriction (Fig. 3 *B* and *E*). In contrast, nifedipine was less effective in the transition zone, where it significantly, but incompletely, relaxed vessels (Fig. 3 *C* and *E*). Nifedipine did not affect the diameter of distal capillaries, despite the fact that these vessels exhibited significant pressure-induced constriction (Fig. 3 *D* and *E*).

To provide additional evidence for the role of VDCCs, we also tested the effects of diltiazem, a specific and potent VDCC inhibitor with a distinct mode of interaction with VDCCs compared with nifedipine (32), applied following nifedipine exposure. Diltiazem had no effect on diameter in nifedipine-pretreated arterioles or capillaries (*SI Appendix*, Fig. S2), lending additional support for the role of VDCCs. These results suggest that sustained constriction in arterioles is dependent on VDCC activity, whereas sustained constriction in capillaries is partially dependent on VDCC activity in the transition zone and completely independent of VDCC activity in distal regions.

Pressure-Induced Ca^{2+} Elevations in Arterioles and Transition Zone/Distal Capillaries. Elevated cytosolic Ca^{2+} concentrations activate myosin light chain kinase, causing contraction of SMCs, and although the contractile machinery that mediates pericyte contraction has not been definitively established, an elevation of cytosolic Ca^{2+} is critical for the contractile behavior of these cells (15, 33, 34). To measure Ca^{2+} responses to pressure changes, we used *Myh11*-GCaMP6f (cre^{ERT2}-loxP) mice, which express the circularly permuted GFP-based Ca^{2+} indicator, GCaMP6f, specifically in SMCs and pericytes under the control of the *Myh11* promoter and show clear GFP fluorescence in all mural cells (4) (Fig. 1 *A* and *C* and *SI Appendix*, Fig. S3). Changes in intracellular Ca^{2+} levels were determined by measuring fluorescence at an inlet pressure of 20 mmHg and after 15 min of sustained inlet pressure elevation to 80 mmHg. Vessels were treated with vehicle [0.005% (v/v) dimethyl sulfoxide] or 500 nM nifedipine, applied 5 min after the pressure change. This protocol, shown in Fig. 4*A*, resulted in a total drug/vehicle exposure of 10 min. Increasing pressure from 20 to 80 mmHg elevated cytosolic Ca^{2+} in arteriolar SMCs and transition zone and distal pericytes (Fig. 4 *B* and *C*). Inhibition of VDCCs with nifedipine abolished pressure-induced elevations of Ca^{2+} in arteriolar SMCs (Fig. 4 *C* and *D*). Nifedipine also reduced Ca^{2+} responses to pressure in transition zone pericytes, although considerable elevation of Ca^{2+} to pressure still persisted (Fig. 4*C*). In contrast to the case for arteriolar SMCs and transition zone pericytes, nifedipine had no effect on pressure-induced Ca^{2+} responses in distal pericytes (Fig. 4*C*). At low, baseline inlet pressure (20 mmHg), exposure to 500 nM nifedipine did not alter cytosolic Ca^{2+} levels in SMCs or pericytes (*SI Appendix*, Fig. S4). A comparison of arteriolar SMCs, transition zone pericytes and distal pericytes demonstrated a zone-specific loss of pressure-induced VDCC-mediated Ca^{2+} responses. Specifically, sustained Ca^{2+} elevations were entirely dependent on VDCC activity in arteriolar SMCs, partially dependent on VDCC activity in transition zone pericytes, and independent of VDCC activity in distal pericytes (Fig. 4*D*).

Next, we utilized the pressure-elevation protocol (Fig. 4*A*) to examine VDCC activity-independent mechanisms of pressure-induced Ca^{2+} in pericytes. Others have reported that pressure-induced Ca^{2+} responses and contraction in vascular SMCs are mediated, in part, by activation of $G_{q/11}$-protein-coupled receptors (G_qPCRs), which activate VDCCs through membrane depolarization (35–37). To examine the mechanisms driving this VDCC-independent Ca^{2+}-influx pathway, we utilized a pharmacological approach. Mechanisms that operate in transition zone pericytes, which also utilize VDCCs, were isolated by performing experiments in the presence of nifedipine.

To test the role of G_qPCRs in VDCC activity-independent elevation of cytosolic Ca^{2+} in pericytes, we used the specific $G_{q/11}$ inhibitor, YM-254890 (38, 39) (YM; 1 μM), a cyclic depsipeptide that prevents guanosine diphosphate release from the G-protein α-subunit. Treatment of a pressurized retina preparation with nifedipine and YM, bath applied at the same time (5 min after elevating pressure from 20 to 80 mmHg) (Fig. 4*A*), resulted in a prominent reduction in pressure-induced Ca^{2+} elevations in transition zone and distal pericytes compared with nifedipine alone (Fig. 4*E*). These observations suggest that G_qPCR activation is a contributor to increases in cytosolic Ca^{2+} in pericytes following pressure elevation.

Membrane potential hyperpolarization relaxes arteriolar SMCs through a reduction in intracellular Ca^{2+} mediated by deactivation of VDCCs (1, 40, 41). In nonexcitable cells, membrane hyperpolarization increases intracellular Ca^{2+} through nonvoltage–dependent Ca^{2+}-entry pathways by virtue of an increase in the electrochemical driving force (42–45). To probe the nature of the Ca^{2+}-entry pathway in pericytes, we applied the adenosine triphosphate-sensitive K^+ (K_{ATP}) channel opener, pinacidil (PIN; 10 μM), which causes approximately a 45-mV hyperpolarization in pericytes (19). In the pressurized retina preparation, treatment with nifedipine and pinacidil, applied at the same time (Fig. 4*A*), resulted in an increase in pressure-induced Ca^{2+} elevation in transition zone and distal pericytes compared with nifedipine alone (Fig. 4*F*). This hyperpolarization-induced increase in pressure-induced Ca^{2+} responses reveal that Ca^{2+} elevation in pericytes is at least partially dependent on Ca^{2+} entry through nonvoltage–dependent ion channels.

One such possible Ca^{2+}-influx pathway is that mediated by plasma membrane transient receptor potential canonical (TRPC) channels, which should exhibit increased Ca^{2+} influx following membrane hyperpolarization because of the increased driving force for Ca^{2+} and the absence of voltage-dependent gating mechanisms (46). These channels play an important role in SMC function and have been implicated in pericyte Ca^{2+} signaling (35, 47–51). We tested whether TRPC channels mediate pressure-induced Ca^{2+} influx in pericytes using the pan-TPRC antagonist, SKF-96365 (SKF; 10 μM). Treatment of a pressurized retina preparation with nifedipine and SKF, applied at the same time (same treatment paradigm as for YM and pinacidil; Fig. 4*A*), resulted in a reduction in pressure-induced Ca^{2+} elevation in transition zone and distal pericytes (Fig. 4*G*), suggesting that TRPC channels participate in Ca^{2+} elevation in pericytes during a sustained pressure stimulus independent of VDCCs.

Taken together, these results suggest that pericyte Ca^{2+} responses to sustained pressure are partially (transition zone) or completely (distal) independent of VDCC activation. Furthermore, this VDCC-independent pathway utilizes G_qPCR signaling and is sustained or initiated, at least in part, through a plasma membrane Ca^{2+} entry pathway that is not voltage gated.

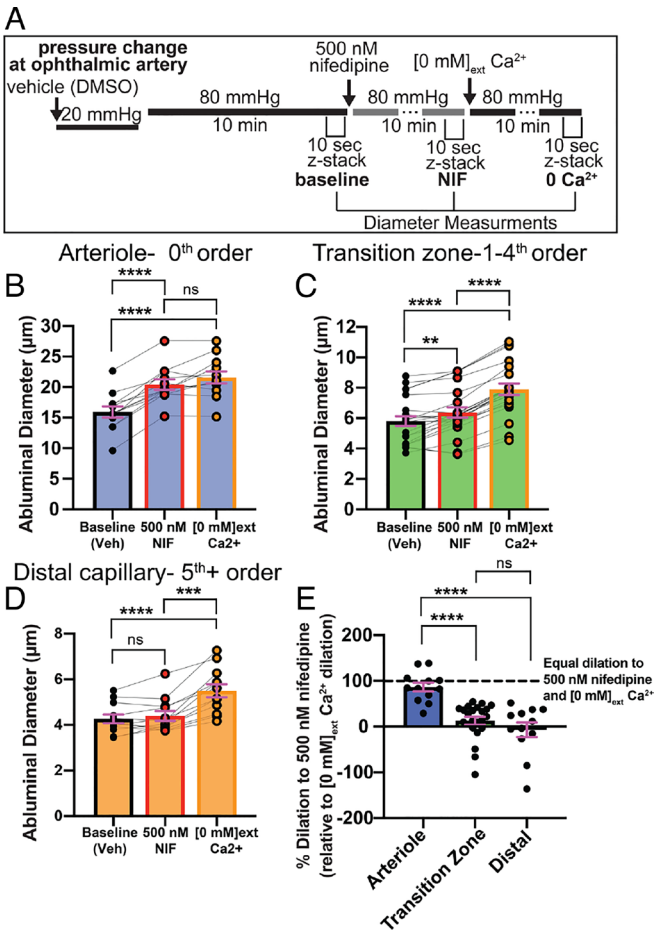

Fig. 3. Pressure-induced dilation of arterioles and capillaries in the presence of nifedipine and [0 mM] external Ca^{2+}. (*A*) Experimental parameters for imaging, pressure changes, and drug applications for sustained-pressure experiments. Baseline diameter at 20 mmHg was determined in the presence of vehicle (0.005% dimethyl sulfoxide [DMSO]). (*B–D*) Abluminal vessel diameter in pressure-constricted arterioles (*B*), transition zone capillaries (*C*), and distal capillaries (*D*) at 80 mmHg, with bath application of 500 nM nifedipine and subsequent exposure to [0 mM] external Ca^{2+} conditions. Data in *B–D* are paired values presented with mean ± SEM (*P < 0.05, **P < 0.01, ***P < 0.001, ****P < 0.0001; one-way ANOVA with Tukey's multiple comparison test); ns, not significant. (*E*) Percent nifedipine-specific dilation (relative to [0 mM] external Ca^{2+} dilation) in arterioles, transition zone capillaries, and distal capillaries (*SI Appendix*, *Methods*). Data are individual values presented with mean ± SEM (n per zone = 8 to 24 from five animals; *P < 0.05, **P < 0.01, ***P < 0.001, ****P < 0.0001; Brown–Forsythe and Welch ANOVA with Welch's correction); ns, not significant.

Zone-Specific Differences in the Time Course of Constriction to Pressure. To determine the time course of arteriole and capillary constriction to pressure, we measured diameter for 10 min following a pressure elevation from 20 to 80 mmHg (Fig. 5*A*). During the first minute following pressure elevation, vessel diameter was measured by performing continuous rapid serial z-stack imaging (Fig. 5*A*). For minutes 2 to 10, vessel diameter was measured by serial z-stack imaging during the last 10 s of every 1-min interval. Only vessels with confirmed constriction at the end of the 10-min period were used for analysis of the temporal properties of constriction. Arteriole constriction was significantly greater than transition zone and distal capillary constriction during the first minute of elevated pressure (Fig. 5 *B* and *C*). Transition zone and distal capillaries constricted on moderate and relatively slow timescales, respectively, following the pressure step; in contrast, arterioles exhibited robust constrictions immediately following pressure elevation (10 to 60 s) that were maintained throughout the 10-min pressure elevation (Fig. 5 *B* and *C*). Since Ca^{2+} elevation is required for constriction in each vascular zone, changes in Ca^{2+} in arteriolar SMCs, transition zone pericytes, and distal pericytes were assessed in the same manner as in Fig. 4, but only rapid changes (1 min after elevating inlet pressure from 20 to 80 mmHg) were evaluated. Arteriolar SMCs, transition zone pericytes, and distal pericytes all exhibited rapid, robust elevations in cytosolic Ca^{2+} following pressure elevation (*SI Appendix*, Fig. S5), responses similar to those observed during sustained pressure elevation (Fig. 4*C*).

These results demonstrate that arteriolar SMCs as well as transition zone and distal pericytes exhibit a rapid rise in cytosolic Ca^{2+} immediately following pressure elevation. Arterioles constrict rapidly to increases in intraluminal pressure, whereas capillaries show differences in constriction kinetics between distal segments (slow) and transition zone segments (intermediate between arterioles and distal pericytes).

Pericytes Depolarize in Response to Increases in Intraluminal Pressure. In arteries and arterioles, increasing intraluminal pressure causes SMC depolarization and Ca^{2+}-dependent constriction through increased Ca^{2+} influx via VDCCs (1, 2). To determine whether this mechanism operates in native pericytes, we investigated the relationship between pressure and membrane voltage in transition zone pericytes (first- to fourth-order vessels) and distal pericytes (fifth-order and above vessels) in our ex vivo pressurized retina preparation using microelectrodes. Pericytes were first identified by their distinct protruding cell body under brightfield illumination (Fig. 6 *A*, first panel). Recorded cell type was verified based on its distance from IEL termination and morphology, visualized by monitoring the fluorescence of 488-hydrazide dye contained in the microelectrode solution that fills the impaled/recorded cell (19) (Fig. 6 *A*, second panel). At low ophthalmic artery pressure (20 mmHg), both transition zone and distal pericytes displayed a membrane potential of approximately −43 mV (−43.6 ± 2.9 mV and −42.1 ± 2.5 mV, respectively); by comparison, retinal SMCs were much more hyperpolarized at this same inlet pressure (membrane potential, −63.8 ± 1.9 mV) (Fig. 6 *B* and *C*), consistent with previous values reported for brain arteriolar SMCs at low, subphysiological pressures (2, 52). Increasing ophthalmic artery pressure from 20 mmHg to 80 mmHg depolarized both transition zone and distal pericytes by ~12 mV (to −31.6 ± 3.3 mV and −30.0 ± 3.3 mV respectively, Fig. 6 *B* and *C*). In contrast, this maneuver depolarized arteriolar SMCs by ~30 mV (to −32.7 ± 0.4 mV) (Fig. 6 *B* and *C*), again a response consistent with those observed in brain arteriolar SMCs upon pressurizing from low or no pressure to a pressure in the physiological range (2, 52). These results reveal a fundamental difference in membrane potential at low pressure between SMCs and pericytes, consistent with a lower K^+ permeability of pericytes relative to SMCs.

VDCC Characteristics in Arteriolar SMCs and Transition Zone/Distal Pericytes. Arterioles constrict robustly at −40 mV (1, 2), a response that is entirely dependent on Ca^{2+} influx through VDCCs in SMCs. In contrast, at the same membrane potential (−40 mV) and a low inlet pressure (20 mmHg; Fig. 6 *B* and *C*), transition zone and distal pericytes showed no loss of contractile or Ca^{2+} responses to application of nifedipine, suggesting relatively low VDCC activity in these cells at this membrane potential (*SI Appendix*, Fig. S4). Furthermore, removal of external Ca^{2+} did not affect vessel diameter at an inlet pressure of 20 mmHg. However, at an inlet pressure of 80 mmHg (about −30 mV), VDCCs did contribute to intracellular Ca^{2+} or contraction of transition zone pericytes, indicating that depolarization from −43 mV to −30 mV activates Ca^{2+} influx through VDCCs.

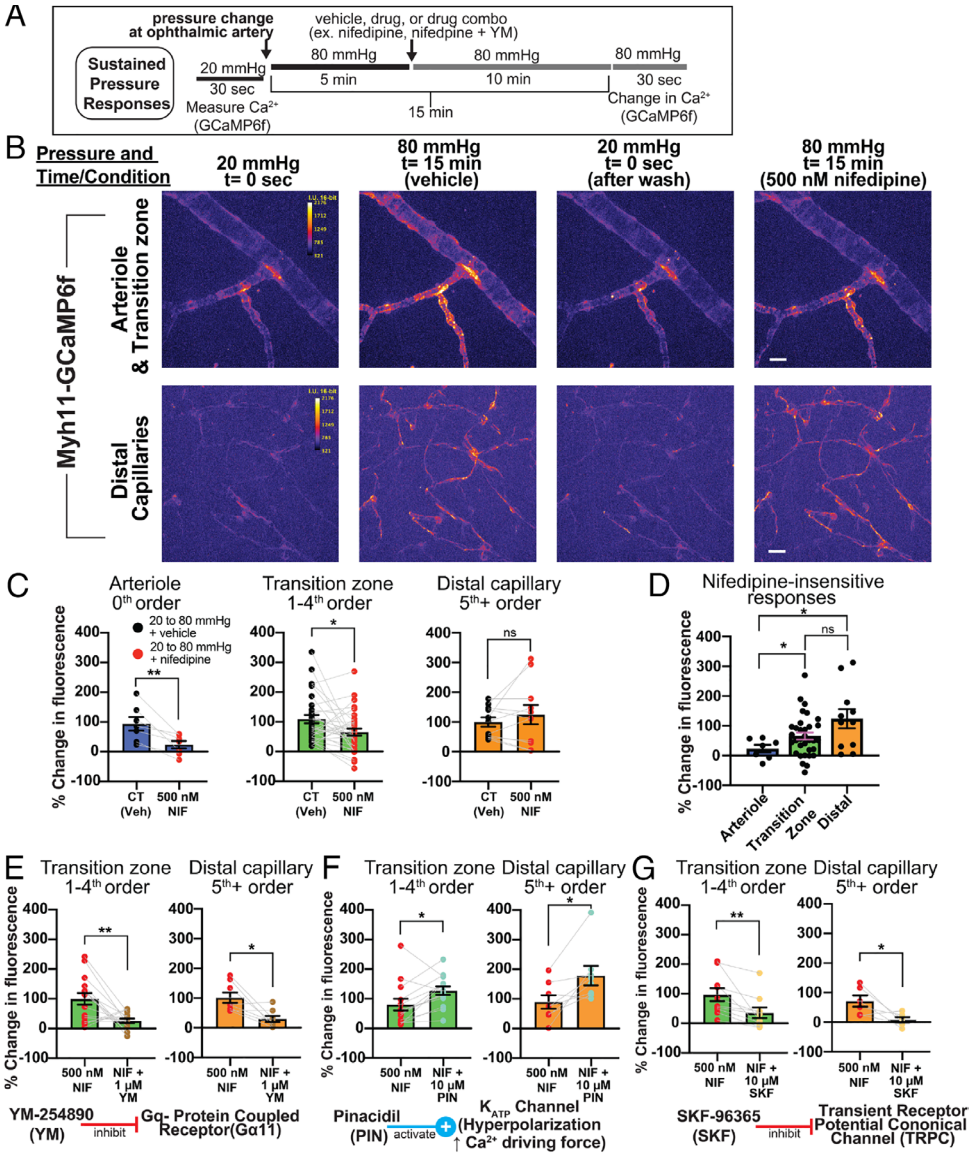

Fig. 4. Sustained Ca^{2+} responses to pressure in arterioles and capillaries. (*A*) Experimental parameters for imaging, pressure changes, and drug applications. Vehicle control, 0.005% for nifedipine alone or 0.1% dimethyl sulfoxide for dual drug treatment. (*B*) First horizontal panel: representative pseudocolored z-projections of arteriole and transition zone capillary GCaMP6f fluorescence at 20 mmHg, 80 mmHg 15 min after pressure change, 20 mmHg (after initial pressure change, return to baseline), and at 80 mmHg 15 min after pressure change with nifedipine (NIF; 10-min treatment), added at 5 min after pressure change. Second horizontal panel: representative image of pseudocolored z-projection of distal capillary pericyte GCaMP6f fluorescence under identical treatment conditions. (Scale bars, 20 μm.) (*C*) Pressure-induced (20 to 80 mmHg at ophthalmic artery) changes in Ca^{2+} (GCaMP6f fluorescence) in arterioles, transition zone capillaries, and distal capillaries with vehicle or 500 nM nifedipine treatment. (*D*) Comparison of nifedipine-insensitive Ca^{2+} changes (500 nM nifedipine) in pressure-stimulated arterioles, transition zone pericytes, and distal pericytes. (*E*) Pressure-induced changes in Ca^{2+} in transition zone capillaries and distal capillaries with 500 nM nifedipine treatment or nifedipine + 1 μM YM-254890. (*F*) Pressure-induced changes in Ca^{2+} in transition zone capillaries and distal capillaries with 500 nM nifedipine treatment or nifedipine + 10 μM pinacidil. (*G*) Pressure-induced changes in Ca^{2+} in transition zone capillaries and distal capillaries with 500 nM nifedipine or nifedipine + 10 μM SKF-96365. Data are individual values presented with mean ± SEM (n = 7 to 24 vessel segments from three to five mice; *C*, *E*, *F*, and *G*: $*P < 0.05$, $**P < 0.01$, paired *t* test; *D*: $*P < 0.05$, $**P < 0.01$; Brown–Forsythe and Welch ANOVA with Welch's correction); ns, not significant.

To test whether functional VDCC channels are activated by depolarization in transition zone and distal pericytes, we exposed *Myh11*-GCaMP6f flat-mount (unpressurized) retina preparations to a depolarizing concentration (60 mM) of external K^+ in the presence and absence of nifedipine. Bath application of 60 mM K^+, which depolarizes vascular cells to approximately −20 mV (1), led to an increase in intracellular Ca^{2+} in all pericytes (and SMCs), effects that were inhibited by nifedipine (500 nM) (Fig. 7 *A* and *B*). This suggests that at membrane potentials around −43 mV, Ca^{2+} influx through VDCC activity is not sufficient to raise Ca^{2+} in pericytes, and that at more depolarized membrane potentials (i.e., −20 mV) sufficient VDCCs are activated to elicit a rise in cytosolic Ca^{2+} in all pericytes.

To directly examine VDCC activity, we measured nifedipine-sensitive currents in native retinal and brain pericytes. Because of experimental limitations in obtaining sufficient numbers of viable single SMCs from retinal arterioles, we compared nifedipine-sensitive VDCC current density between SMCs and pericytes using cells isolated from cortical brain tissue. The identification of single pericytes was aided by the use of NG2-DsRed-BAC transgenic mice, in which expression of the DsRed fluorescent protein is driven by the promoter region of the chondroitin sulfate proteoglycan 4 (*Cspg4*) gene encoding the mural cell marker, neural/glial antigen 2 (NG2) (19). Isolated pericytes exhibited a characteristic outward protruding nucleus with long-stranded projections. To maximize channel open probability and decrease inactivation, we bathed native pericytes in a solution

containing the VDCC activator, Bay K 8644 (500 nM), together with 10 mM Ba^{2+}. In pericytes and SMCs held at −60 mV, a 200-ms −90-mV prepulse followed by a 300-ms voltage step to +10 mV evoked an inward, nifedipine-sensitive current (Fig. 7*C*). The amplitudes of nifedipine-subtracted currents in brain (−4.6 ± 1.2 pA/pF) and retinal (−4.1 ± 0.4 pA/pF) pericytes were comparable (Fig. 7 *C* and *E*) but were approximately half that of currents recorded in single cerebral pial artery SMCs (−8.9 ± 0.5 pA/pF; Fig. 7 *D* and *E*. Overall, these results indicate that, although pericytes utilize mechanisms independent of VDCCs to elevate Ca^{2+} during pressure elevation, both transition zone and distal pericytes possess functional VDCCs.

Discussion

Here, we tested the postulate that pressure is an intrinsic stimulus that establishes baseline contractility, or "tone," in CNS pericytes and may contribute to pressure-sensitive autoregulation within the capillary network. The intrinsic ability of blood vessels to constrict in response to increases in systemic pressure, a mechanism that serves to maintain stable blood flow, was first described empirically in the early 20th century (53) and was subsequently appreciated to apply to the CNS vasculature (54). Long-standing interest in the detailed mechanisms that govern this pressure-induced constriction, or myogenic response, has continued to drive efforts to better understand blood flow regulation under healthy and diseased conditions. Recent studies have identified a population of morphologically distinct pericytes in the capillary transition zone that display relatively rapid, Ca^{2+}-dependent contractile properties and the ability to dynamically control capillary blood flow (4–7, 12). We are only beginning to understand the impact of distal pericytes on cerebral blood flow regulation, but clearly contractile/relaxation kinetics and mechanisms of this subpopulation differ from those of SMCs and proximal transition zone pericytes (5, 15). Although the physiological mechanisms that mediate Ca^{2+} responses and contractility in pericytes are often presumed to be similar or identical to those of SMCs, they remain empirically undefined.

Utilizing a pressurized retina preparation, we demonstrate that arterioles, transition zone capillaries, and distal capillaries constrict or maintain their intraluminal diameters in response to increasing perfusion pressure, thus providing a mechanism for establishing vascular tone and stabilizing downstream capillary blood flow. The kinetics of this contractile behavior are distinct in each vascular zone, such that arterioles and transition zone capillaries generate tone more rapidly than distal capillaries. Moreover, the mechanisms that regulate intracellular Ca^{2+} and contractility along the arteriole-capillary continuum display a unique, zone-specific gradient in their reliance on VDCC activity. Specifically, SMCs are entirely dependent on VDCC activity for sustained contraction, whereas contraction of transition zone pericytes is only partially dependent on VDCCs and distal pericyte contraction does not depend on VDCC activity at all. The distinct features of each vascular zone are highlighted in Fig. 8.

These results underscore the potential for all pericytes to contribute to the regulation of capillary blood flow in response to changing pressure through their distinct temporal and Ca^{2+}-influx properties. One postulate arising from these results is that intraluminal pressure per se is a unique mechanism for preconstricting pericytes and thus establishing a baseline constriction from which dynamic or static flow properties can vary.

Our results support the idea that, in addition to SMCs, all pericytes possess VDCCs. A major difference is the membrane potential at which Ca^{2+} entry is sufficient to cause a detectable increase in intracellular Ca^{2+} and constriction, particularly in transition zone capillaries. Indeed, at subphysiological inlet pressures

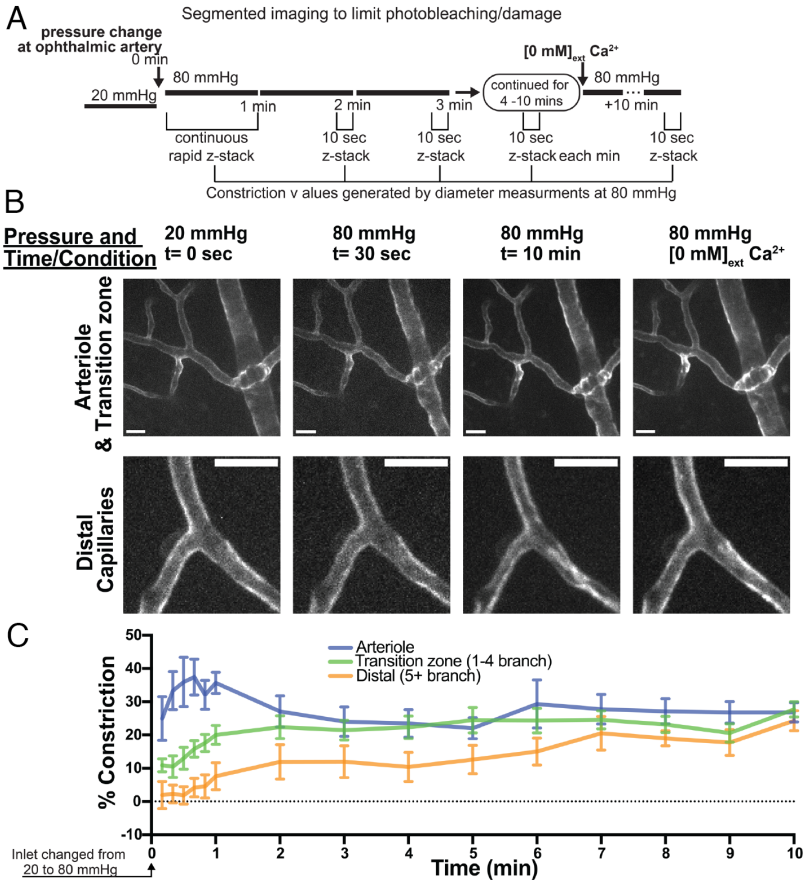

Fig. 5. Temporal properties of pressure-induced constriction in arterioles and capillaries. (*A*) Experimental parameters for pressure change and imaging. (*B*) Representative images of arterioles, transition zone capillaries, and distal capillaries at 20 mmHg (0 s), at 80 mmHg for 30 s and 10 min, and passively dilated at 80 mmHg. Only vessels with confirmed constriction at the end of 10 min were used for analysis of temporal properties of constriction. (Scale bars, 20 um.) (*C*) Percent constriction developed in different zones over 10 min following pressure elevation (20 to 80 mmHg). Data are mean ± SEM (n per branch = 5 to 11 from five animals; $P < 0.0001$ for differences in constriction among the three groups at 1 min, two-way ANOVA with Tukey's multiple comparison test).

(20 mmHg at the ophthalmic artery), pericytes are substantially depolarized (approximately −43 mV) relative to SMCs (approximately −60 mV) and possess the capacity to depolarize further (to −30 mV) in response physiological intraluminal pressures. However, inhibiting VDCCs in pericytes at low pressure (associated with a membrane potential of −40 mV) did not alter pericyte diameter or Ca^{2+} levels; by contrast, parenchymal arterioles constrict robustly between −50 and −40 mV (1, 2). Inhibiting VDCCs at physiological pressures (associated with an SMC and pericyte membrane potential of approximately −30 mV) leads to dilation of arterioles and transition zone capillaries, suggesting that this membrane potential is sufficient for VDCC activation and contraction in these cells. However, distal pericytes, which constrict at physiological pressures (at −30 mV), did not dilate during VDCC inhibition, suggesting that VDCC activity is not a primary mechanism for Ca^{2+} elevation at this pressure/membrane potential. In fact, in our previous study, we demonstrated that sustained exposure to further depolarized conditions (membrane potential ≈ −20 mV) by addition of 60 mM extracellular K^+ is unable to contract distal pericytes (4). Although the properties of VDCCs (e.g., current density) in pericytes, particularly transition zone pericytes, need further characterization, the difference between SMCs and pericytes may reside in the lower current density of VDCCs in pericytes. A detailed account of VDCC properties, including voltage dependence of activation and inactivation, cooperative gating, and direct/indirect modulation by phosphorylation or other regulatory proteins, is needed to fully understand differences in VDCCs in pericytes versus those in SMCs.

Interestingly, in contrast to the lack of 60 mM K^+ constriction responses in distal pericytes mentioned above, we showed that sustained exposure to the G_qPCR agonist, U-46619, which acts at the thromboxane A2 receptor, was able to evoke constriction in distal capillaries (4). Together, these results indicate that pericytes may utilize a mechanism independent of VDCC activity to sustain contraction. Previous studies examining SMCs show that G_qPCR stimulation and subsequent activation of nonselective cation channels, such as Transient Receptor Potential Cation Channel Subfamily M Member 4 (TRPM4) and TRPC channels, provides depolarization for sustained VDCC activity and contractility (35–37, 49, 55). In transition zone pericytes, G_qPCR activation of these cation channels may create depolarizing conditions for VDCC activity and provide a VDCC-independent Ca^{2+} source, which combine to promote contractility in these cells. In distal pericytes, sustained G_qPCR activation of other types of Ca^{2+}-permeable channels may provide the predominant Ca^{2+} source for initiation of contraction. Indeed, we found that, in the presence of nifedipine, G_qPCR inhibitors reduced pressure-induced Ca^{2+} elevations in both transition zone and distal pericytes, whereas nifedipine alone abolished Ca^{2+} elevations in arteriolar SMCs. Furthermore, in the absence of VDCC activity, pressure-induced Ca^{2+} elevation is enhanced through hyperpolarization-induced increases in the driving force for Ca^{2+}. This suggests that Ca^{2+} influx through nonvoltage–gated, Ca^{2+}-permeable channels is a key contributor to Ca^{2+}-mediated contraction of pericytes. To specifically examine VDCC-independent mechanisms, in these experiments we exposed the entire preparation to nifedipine, a maneuver that was especially important in examining transition zone pericytes, in which sustained contraction is partially dependent on VDCC activity. An important caveat to bear in mind in considering these results is potential cross-talk between VDCCs and other Ca^{2+} entry/release pathways, a possibility that cannot be ruled out. We did not explore contributions of store release to Ca^{2+} elevation in pericytes, specifically the role of inositol 1,3,5-triphosphate (IP_3) receptors, which have known signaling roles in pericytes (4) and are canonical downstream targets of the GqPCR-phospholipase C-diacylglycerol/IP_3 signaling cascade. Although IP_3 receptor function is not necessary for sustained Ca^{2+} elevation and contraction of SMCs (56), Ca^{2+} release may have a more prominent role in

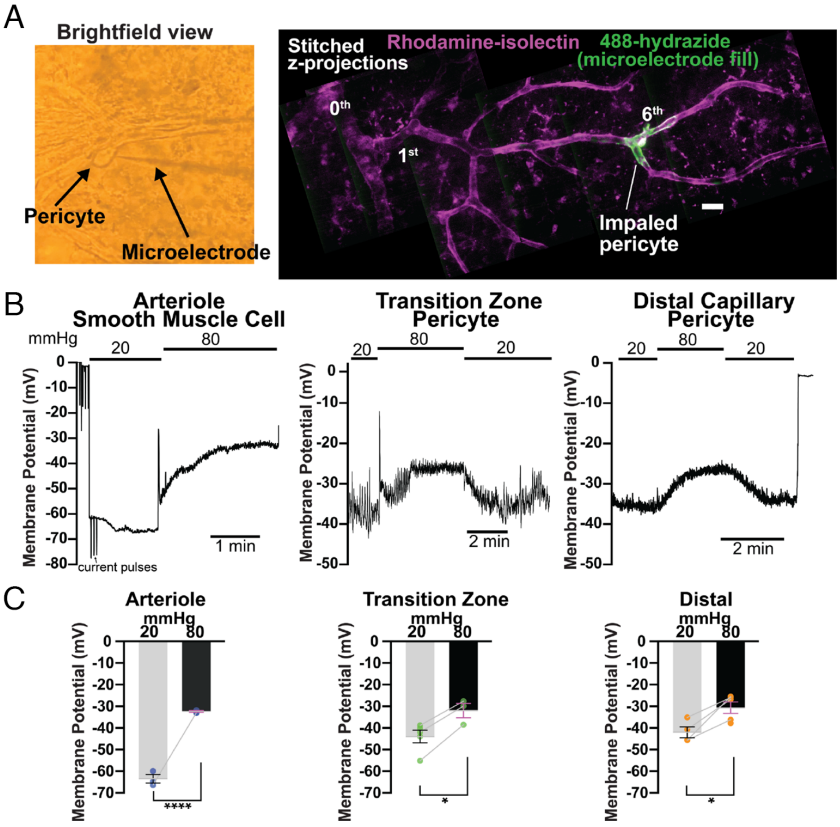

Fig. 6. Pericyte membrane potential responses to changes in pressure. (*A*) First panel, localization, and identification of pericytes. Pericytes within the pressurized retinal vasculature were first identified by brightfield microscopy and then impaled with microelectrodes. Second panel, hydrazide-filled pericytes, imaged following impalement and membrane potential recordings to confirm pericyte morphology and location (branch order). The vasculature was also stained with rhodamine-isolectin (magenta) to highlight branching structure. (Scale bar, 20 μm.) (*B*) Membrane potential responses to stepped pressure changes (from 20 to 80 mmHg), recorded from an arteriolar SMC, transition zone (second-order) pericyte, and distal (sixth-order) pericyte. All changes in pressure were measured at the ophthalmic artery. (*C*) Summary data showing membrane potential in arteriolar SMCs (blue), transition zone pericytes (green), and distal pericytes (orange) at ophthalmic artery pressures of 20 and 80 mmHg. Data are paired and unpaired individual values presented with mean ± SEM [n = 3 SMCs from three mice and n = 3 to 4 pericytes per zone from three to four mice; **P* < 0.05, ***P* < 0.01, ****P* < 0.001, *****P* < 0.0001, unpaired *t* test for SMCs and transition zone pericytes (unpaired values at 20 and 80 mmHg for arterioles and two unpaired values at 20 mmHg for transition zone pericytes) and paired *t* test for distal pericytes].

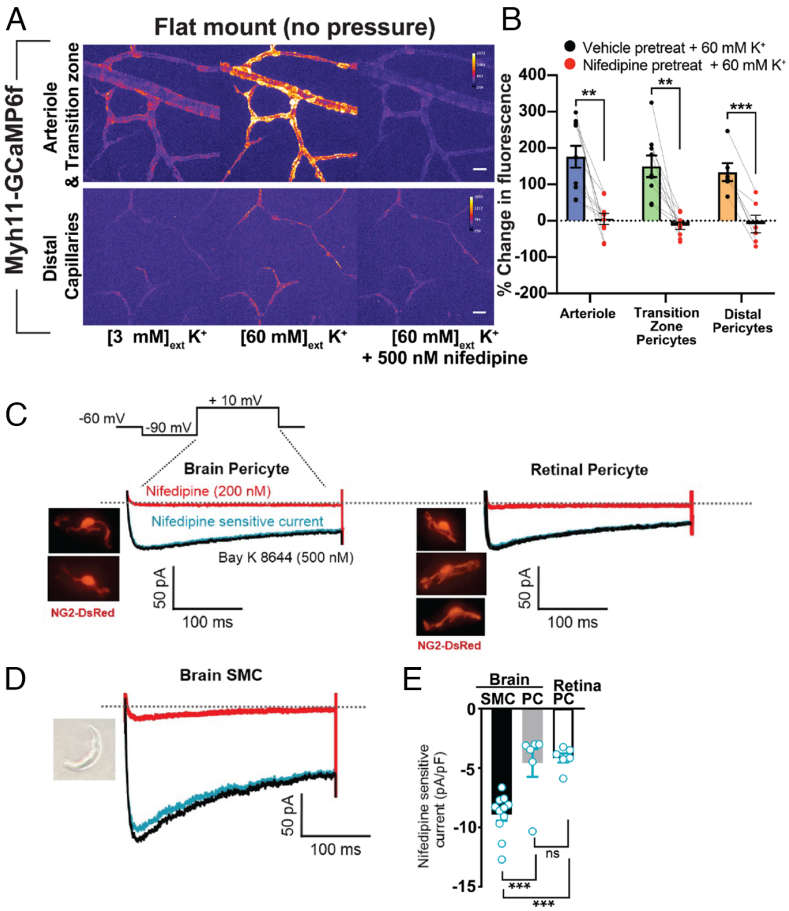

Fig. 7. Functional expression of VDCCs in pericytes. (*A*) Representative pseudocolored image of GCaMP6f fluorescence in flat-mount retinal arterioles, transition zone capillaries, and distal capillaries in 3 mM external K^+ (normal) 60 mM external K^+, or 60 mM external K^+ with pretreatment with 500 nM nifedipine. (Scale bars, 20 μm.) (*B*) Summary data showing Ca^{2+} levels (change in GCaMP6f fluorescence values) in arterioles and transition zone and distal capillaries in response to a depolarizing (60 mM) concentration of external K^+ without (vehicle) and with 500 nM nifedipine pretreatment. Data are paired individual values with mean ± SEM (n = 6 to 10 vessels per zone from four to five animals; $*P < 0.05$, $**P < 0.01$, $***P < 0.001$, paired *t* test). (*C*) Voltage step protocol used for all whole-cell recordings (*SI Appendix, Methods*). Representative images and current traces from isolated native cerebral and retinal pericytes from NG2-DsRed mice, recorded in the presence of the VDCC agonist Bay K 8644 (500 nM) or antagonist nifedipine (200 nM). Blue trace: subtracted (nifedipine-sensitive) current. (*D*) Representative image and current traces from isolated cerebral SMC under the same conditions as *C*. (*E*) Summary data showing current density for subtracted current conditions in isolated SMCs, brain pericytes, and retinal pericytes. Data are unpaired individual values with mean ± SEM (n = 6 to 11 per cell type from two to three animals; $*P < 0.05$, $**P < 0.01$, $***P < 0.001$, Brown–Forsythe and Welch ANOVA with Welch's correction); ns, not significant.

pericytes, and in particular distal pericytes. It is apparent that an extracellular Ca^{2+} source is required for contraction. However, this could reflect Ca^{2+} activation of IP_3 receptors and maintenance of luminal Ca^{2+} in the endoplasmic reticulum.

SMC membrane potential is a powerful regulator of arterial and arteriolar diameter and blood flow. The transducer is the VDCC, which exhibits a steep increase in open probability with membrane potential depolarization (56). Indeed, drugs that hyperpolarize smooth muscle are powerful vasodilators (57). The lack of a functional role of VDCCs in distal pericytes indicate that this mechanism is not operational in response to pressure in distal pericytes (58). Indeed, pinacidil, which causes hyperpolarization by activation of K_{ATP} channels, causes an increase in pressure-induced Ca^{2+} responses in distal pericytes. Theoretically, physiological hyperpolarization in the distal capillary network could promote pericyte contraction through enhanced Ca^{2+} entry while dilating upstream vessels through retrograde hyperpolarization (28). Another intriguing rationale for relatively depolarized membrane potentials of pericytes at low and physiological pressures is to maintain the ability to hyperpolarize during physiological stimuli such as neuronal activity or dilatory ligand release, allowing for transmission of hyperpolarization to underlying endothelial cells (19, 28, 59).

A limitation of the pressurized retina preparation, or any in vivo or ex vivo intact flow system (60), is the inability to definitively know the exact pressure within each downstream microvascular zone. However, pressurizing the ophthalmic artery to physiological levels likely provides a physiologically relevant pressure drop along the branching vascular tissue. This inference is supported by the observation of intact flow from arterioles to capillaries to venules, and the demonstration of physiological flow rates in draining vessels in the retina preparation. This is reliably achieved by cannulating and pressurizing at a site several millimeters distal from the retinal arterioles and allowing the natural inlet arteries (ophthalmic artery and retinal artery) to initially regulate flow generated through a known pressure. This is in contrast to the pressurized brain slice preparation, in which arterioles are directly cannulated with the connected vasculature, and careful flow calibration at respective inlet pressures is required (61–63). Nevertheless, pressures along the arteriole-capillary axis certainly fall dramatically in a branching, intact-flow systems, where pressure in the distal capillaries is probably less than 20 mmHg (60). It is likely that pressures encountered in each vascular zone change as a function of time following pressure elevation, especially given the rapid constriction of arterioles. Even though SMCs, transition zone pericytes, and distal pericytes all show an immediate, substantial elevation in Ca^{2+} that is sustained following pressure elevation, the potential impacts of these fluctuations as the preparation reaches equilibration should be considered when interpreting these results.

Although the intraluminal pressure within capillaries is much lower than upstream vessels, capillaries still constrict in response to a pressure stimulus. This is likely a feature of microvessels, where smaller vessels generate meaningful tone at much lower intraluminal pressures, as exemplified by the 30 to 40% tone generated at 80 mmHg in brain pial arteries versus the same degree of tone generated in downstream penetrating arterioles at 40 mmHg (1, 2, 49, 52). Another aspect of capillary constriction not directly explored in this study is the force required to generate meaningful constriction in the arteriole versus capillary segments. Arterioles experience considerably higher intraluminal pressures and also contain a layer of elastin. These factors require that SMCs generate much greater contractile forces to regulate diameter and flow rapidly and dynamically. In contrast, pericytes share a basement membrane with underlying endothelial cells and experience lower intraluminal pressures. The relatively low-pressure environment and projection nature of pericyte coverage may not require such

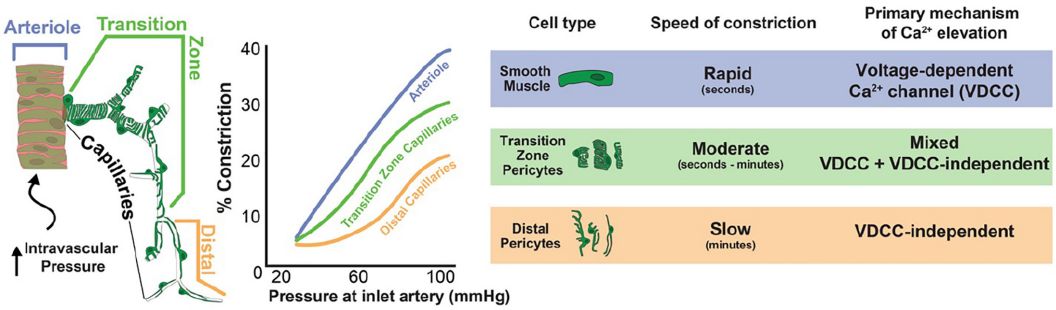

Fig. 8. Pressure-induced constriction along the arteriole-capillary continuum. Schematic illustrates the zonal distribution and morphology of SMCs and pericytes along the arteriole-capillary continuum. Each vascular zone responds differently to increased inlet pressure at the ophthalmic artery. The involvement of VDCCs in pressure-induced constriction is dependent on cell type, with complete or partial involvement in SMCs and transition zone pericytes respectively, and no involvement in distal pericytes.

robust excitation–contraction coupling mechanisms, such as the exclusive reliance on VDCC activity or high levels of αSMA. Nevertheless, SMCs and transition zone and distal pericytes all exhibit a relatively immediate (~1 min or less) depolarization (Fig. 6) and Ca^{2+} elevation (Fig. 6 and *SI Appendix*, Fig. S5) to pressure, yet the speed of their constriction is distinct in each zone. This may indicate zone-specific relationships between cytosolic Ca^{2+} concentration in the cells and the rate at which these concentrations translate to meaningful force production. These results also indicate that the timing of depolarization aligns fairly well with the contractile response in cells that utilize VDCCs for contraction (i.e., SMCs and transition zone pericytes). They also raise an intriguing question: What is the effect of depolarization in distal pericytes and what are implications of this process for pressure sensing? Ultimately the biophysical and biomechanical nature of pericyte contraction warrants future investigation.

Additionally, the interconnected nature of all pressurized vessels in this preparation means that downstream capillaries are subjected to pressure-change effects contributed by upstream arterioles and early capillary branches. However, for several reasons, it is unlikely that these results reflect passive responses to upstream vessels. First, substantial arteriole contractile responses occur in seconds, whereas significant changes in distal capillaries occur after minutes. Second, inhibition of VDCCs causes complete relaxation of upstream arterioles with no effect on pressure-constricted distal capillaries. And third, pressure leads to a rapid and pronounced increase in pericyte Ca^{2+} signals, which are sustained and required for contraction, indicating that pericytes sense increases in pressure.

Taken together, these observations highlight the unique contractile mechanisms in pericytes and may explain cases where "canonical" vasodilatory signals that lead to hyperpolarization and modulation of VDCC activity have different dilatory effects along the capillary continuum. It may also explain why other mediators/stimuli appear to cause distinct, but slow, dilation of distal pericytes (15), as these mechanisms might inhibit VDCC-independent Ca^{2+}-entry and/or release pathways, processes that could be slower than modulation of voltage-dependent channels.

Materials and Methods

All animals were used in accordance with protocols approved by the Institutional Animal Care and Use Committee of the University of Vermont. Detailed description of animal procedures and strains including myh11-Cre^{ERT2} mice [courtesy of Stefan Offermans (64)] are included in *SI Appendix, Methods*. Details for procedures and materials required for pressurized ex vivo retina preparation, immunohistochemistry, vessel diameter and Ca^{2+} imaging, fluorescent bead imaging, membrane potential and patch clamp electrophysiology are included in *SI Appendix, Methods*.

Statistical Analysis. Data are expressed as paired or unpaired individual values with mean ± standard error of the sample mean (SEM). Datasets were tested for normal distribution using the D'Agostino and Pearson test. Normally distributed data were evaluated using appropriate parametric statistical tests, whereas nonnormally distributed (i.e., non-Gaussian) datasets were tested using appropriate nonparametric statistical tests. Individual statistical tests are indicted in the corresponding figure legend. GraphPad Prism 9 software was used for statistical analysis. A *P*-value less than 0.05 considered statistically significant; individual *P*-value thresholds (*$P < 0.05$, **$P < 0.01$, ***$P < 0.001$, ****$P < 0.0001$) are indicated in figure legends.

Data, Materials, and Software Availability. All study data are included in the article and/or *SI Appendix*.

ACKNOWLEDGMENTS. We thank N. Labinger and A. Hepp for experimental assistance; T. Wellman and D. Enders for technical assistance and animal care; G. Hennig, N. Tsoukias, A. Joutel and A. Bonev for conceptual and technical feedback; and T. Clason for microscopy assistance. This study was supported by grants from the Totman Medical Research Trust, the European Union (Horizon 2020 Research and Innovation Programme SVDs@target under grant agreement 666881), The Cardiovascular Research Institute of Vermont to N.R.K., and the NIH [F32HL152576 to N.R.K.; K01HL138215 and P20GM130459 to A.L.G.; P20GM135007, RF1NS128963, R01NS110656 and R35HL140027 to M.T.N; and R01NS119971 to Nikolaos Tsoukias (subcontract to M.T.N.)].

Author affiliations: [a]Department of Pharmacology, Larner College of Medicine, University of Vermont, Burlington, VT 05405; [b]Department of Physiology and Cell Biology, School of Medicine, University of Nevada, Reno, NV 89557; and [c]Division of Cardiovascular Sciences, University of Manchester, Manchester M13 9PL, UK

1. H. J. Knot, M. T. Nelson, Regulation of arterial diameter and wall [Ca2+] in cerebral arteries of rat by membrane potential and intravascular pressure. *J. Physiol.* **508**, 199–209 (1998).
2. M. A. Nystoriak *et al.*, Fundamental increase in pressure-dependent constriction of brain parenchymal arterioles from subarachnoid hemorrhage model rats due to membrane depolarization. *Am. J. Physiol. Heart Circ. Physiol.* **300**, H803–H812 (2011).
3. J. Claassen *et al.*, Regulation of cerebral blood flow in humans: Physiology and clinical implications of autoregulation. *Physiol. Rev.* **101**, 1487–1559 (2021).
4. A. L. Gonzales *et al.*, Contractile pericytes determine the direction of blood flow at capillary junctions. *Proc. Natl. Acad. Sci. U.S.A.* **117**, 27022–27033 (2020).
5. R. L. Rungta *et al.*, Vascular compartmentalization of functional hyperemia from the synapse to the pia. *Neuron* **99**, 362–375.e4 (2018).
6. C. Cai *et al.*, Stimulation-induced increases in cerebral blood flow and local capillary vasoconstriction depend on conducted vascular responses. *Proc. Natl. Acad. Sci. U.S.A.* **115**, E5796–E5804 (2018).
7. C. N. Hall *et al.*, Capillary pericytes regulate cerebral blood flow in health and disease. *Nature* **508**, 55–60 (2014).
8. D. A. Hartmann, V. Coelho-Santos, A. Y. Shih, Pericyte control of blood flow across microvascular zones in the central nervous system. *Annu. Rev. Physiol.* **84**, 331–354 (2021).

9. R. I. Grant *et al.*, Organizational hierarchy and structural diversity of microvascular pericytes in adult mouse cortex. *J. Cereb. Blood Flow Metab.* **39**, 411–425 (2019).
10. C. M. Peppiatt *et al.*, Bidirectional control of CNS capillary diameter by pericytes. *Nature* **443**, 700–704 (2006).
11. N. B. Hamilton, D. Attwell, C. N. Hall, Pericyte-mediated regulation of capillary diameter: A component of neurovascular coupling in health and disease. *Front Neuroenergetics* **2**, 5 (2010).
12. S. Grubb *et al.*, Precapillary sphincters maintain perfusion in the cerebral cortex. *Nat. Commun.* **11**, 395 (2020).
13. M. Vanlandewijck *et al.*, A molecular atlas of cell types and zonation in the brain vasculature. *Nature* **554**, 475–480 (2018).
14. K. Sakagami, D. M. Wu, D. G. Puro, Physiology of rat retinal pericytes: Modulation of ion channel activity by serum-derived molecules. *J. Physiol.* **521**, 637–650 (1999).
15. D. A. Hartmann *et al.*, Brain capillary pericytes exert a substantial but slow influence on blood flow. *Nat. Neurosci.* **24**, 633–645 (2021).
16. A. R. Nelson *et al.*, Channelrhodopsin excitation contracts brain pericytes and reduces blood flow in the aging mouse brain in vivo. *Front. Aging Neurosci.* **12**, 108 (2020).
17. R. Nortley *et al.*, Amyloid beta oligomers constrict human capillaries in Alzheimer's disease via signaling to pericytes. *Science* **365**, eaav9518 (2019).
18. J. Ratelade *et al.*, Reducing hypermuscularization of the transitional segment between arterioles and capillaries protects against spontaneous intracerebral hemorrhage. *Circulation* **141**, 2078–2094 (2020).
19. M. Sancho *et al.*, Adenosine signaling activates ATP-sensitive K(+) channels in endothelial cells and pericytes in CNS capillaries. *Sci. Signal* **15**, eabl5405 (2022).
20. O. F. Harraz *et al.*, Piezo1 is a mechanosensor channel in central nervous system capillaries. *Circ. Res.* **130**, 1531–1546 (2022).
21. B. P. Peters, I. J. Goldstein, The use of fluorescein-conjugated Bandeiraea simplicifolia B4-isolectin as a histochemical reagent for the detection of alpha-D-galactopyranosyl groups. Their occurrence in basement membranes. *Exp. Cell Res.* **120**, 321–334 (1979).
22. Z. Shen *et al.*, An artery-specific fluorescent dye for studying neurovascular coupling. *Nat. Methods* **9**, 273–276 (2012).
23. P. S. Clifford *et al.*, Spatial distribution and mechanical function of elastin in resistance arteries: A role in bearing longitudinal stress. *Arterioscler. Thromb. Vasc. Biol.* **31**, 2889–2896 (2011).
24. D. A. Hartmann *et al.*, Pericyte structure and distribution in the cerebral cortex revealed by high-resolution imaging of transgenic mice. *Neurophotonics* **2**, 041402 (2015).
25. M. R. Glucksberg, R. Dunn, Direct measurement of retinal microvascular pressures in the live, anesthetized cat. *Microvasc. Res.* **45**, 158–165 (1993).
26. C. J. Pournaras *et al.*, Regulation of retinal blood flow in health and disease. *Prog. Retin. Eye Res.* **27**, 284–330 (2008).
27. S. S. Hayreh, J. Edwards, Ophthalmic arterial and venous pressures. Effects of acute intracranial hypertension. *Br. J. Ophthalmol.* **55**, 649–663 (1971).
28. T. A. Longden *et al.*, Capillary K(+)-sensing initiates retrograde hyperpolarization to increase local cerebral blood flow. *Nat. Neurosci.* **20**, 717–726 (2017).
29. A. Mishra, A. Hamid, E. A. Newman, Oxygen modulation of neurovascular coupling in the retina. *Proc. Natl. Acad. Sci. U.S.A.* **108**, 17827–17831 (2011).
30. S. H. Nellis, B. W. Zweifach, A method for determining segmental resistances in the microcirculation from pressure-flow measurements. *Circ. Res.* **40**, 546–556 (1977).
31. A. Joseph, A. Guevara-Torres, J. Schallek, Imaging single-cell blood flow in the smallest to largest vessels in the living retina. *Elife* **8**, e45077 (2019).
32. L. Tang *et al.*, Structural basis for diltiazem block of a voltage-gated Ca(2+) channel. *Mol. Pharmacol.* **96**, 485–492 (2019).
33. L. Jin, Z. Ying, R. C. Webb, Activation of Rho/Rho kinase signaling pathway by reactive oxygen species in rat aorta. *Am. J. Physiol. Heart Circ. Physiol.* **287**, H1495–H1500 (2004).
34. Y. Fukata, M. Amano, K. Kaibuchi, Rho-Rho-kinase pathway in smooth muscle contraction and cytoskeletal reorganization of non-muscle cells. *Trends Pharmacol. Sci.* **22**, 32–39 (2001).
35. M. Mederos y Schnitzler *et al.*, Gq-coupled receptors as mechanosensors mediating myogenic vasoconstriction. *EMBO J.* **27**, 3092–3103 (2008).
36. J. Schleifenbaum *et al.*, Stretch-activation of angiotensin II type 1a receptors contributes to the myogenic response of mouse mesenteric and renal arteries. *Circ. Res.* **115**, 263–272 (2014).
37. P. W. Pires *et al.*, The angiotensin II receptor type 1b is the primary sensor of intraluminal pressure in cerebral artery smooth muscle cells. *J. Physiol.* **595**, 4735–4753 (2017).
38. J. Takasaki *et al.*, A novel Galphaq/11-selective inhibitor. *J. Biol. Chem.* **279**, 47438–47445 (2004).
39. J. Patt *et al.*, An experimental strategy to probe Gq contribution to signal transduction in living cells. *J. Biol. Chem.* **296**, 100472 (2021).
40. J. M. Quayle *et al.*, Single calcium channels in resistance-sized cerebral arteries from rats. *Am. J. Physiol.* **264**, H470–H478 (1993).
41. M. Rubart, J. B. Patlak, M. T. Nelson, Ca2+ currents in cerebral artery smooth muscle cells of rat at physiological Ca2+ concentrations. *J. Gen. Physiol.* **107**, 459–472 (1996).
42. T. A. Longden *et al.*, Local IP3 receptor-mediated Ca(2+) signals compound to direct blood flow in brain capillaries. *Sci. Adv.* **7**, eabh0101 (2021).
43. K. A. Dora, C. J. Garland, Linking hyperpolarization to endothelial cell calcium events in arterioles. *Microcirculation* **20**, 248–256 (2013).
44. E. J. Behringer, S. S. Segal, Membrane potential governs calcium influx into microvascular endothelium: Integral role for muscarinic receptor activation. *J. Physiol.* **593**, 4531–4548 (2015).
45. H. J. Knot, K. M. Lounsbury, J. E. Brayden, M. T. Nelson, Gender differences in coronary artery diameter reflect changes in both endothelial Ca2+ and ecNOS activity. *Am J Physiol.* **276**, H961–H969 (1999).
46. V. Flockerzi, An introduction on TRP channels. *Handb. Exp. Pharmacol.* **179**, 1–19 (2007).
47. A. L. Gonzales *et al.*, A PLCgamma1-dependent, force-sensitive signaling network in the myogenic constriction of cerebral arteries. *Sci. Signal.* **7**, ra49 (2014).
48. J. Narayanan *et al.*, Pressurization of isolated renal arteries increases inositol trisphosphate and diacylglycerol. *Am. J. Physiol.* **266**, H1840–H1845 (1994).
49. G. Osol, I. Laher, M. Kelley, Myogenic tone is coupled to phospholipase C and G protein activation in small cerebral arteries. *Am. J. Physiol.* **265**, H415–H420 (1993).
50. S. Earley, S. V. Straub, J. E. Brayden, Protein kinase C regulates vascular myogenic tone through activation of TRPM4. *Am. J. Physiol. Heart Circ. Physiol.* **292**, H2613–H2622 (2007).
51. Y. T. Xuan, O. L. Wang, A. R. Whorton, Regulation of endothelin-induced Ca2+ mobilization in smooth muscle cells by protein kinase C. *Am. J. Physiol.* **266**, C1560–C1567 (1994).
52. F. Dabertrand *et al.*, Potassium channelopathy-like defect underlies early-stage cerebrovascular dysfunction in a genetic model of small vessel disease. *Proc. Natl. Acad. Sci. U.S.A.* **112**, E796–E805 (2015).
53. W. M. Bayliss, On the local reactions of the arterial wall to changes of internal pressure. *J. Physiol.* **28**, 220–231 (1902).
54. M. Fog, The relationship between the blood pressure and the tonic regulation of the pial arteries. *J. Neurol. Psychiatry* **1**, 187–197 (1938).
55. U. Storch, M. Mederos y Schnitzler, T. Gudermann, G protein-mediated stretch reception. *Am. J. Physiol. Heart Circ. Physiol.* **302**, H1241–H1249 (2012).
56. M. T. Nelson *et al.*, Calcium channels, potassium channels, and voltage dependence of arterial smooth muscle tone. *Am. J. Physiol.* **259**, C3–C18 (1990).
57. N. B. Standen *et al.*, Hyperpolarizing vasodilators activate ATP-sensitive K+ channels in arterial smooth muscle. *Science* **245**, 177–180 (1989).
58. C. Gluck *et al.*, Distinct signatures of calcium activity in brain mural cells. *Elife.* **10**, e70591 (2021).
59. A. Hariharan *et al.*, Brain capillary pericytes are metabolic sentinels that control blood flow through K_{ATP} channel-dependent energy switch. *Cell Rep.* **41**, 111872 (2022). https://doi.org/doi:10.1016/j.celrep.2022.111872.
60. F. Schmid *et al.*, Depth-dependent flow and pressure characteristics in cortical microvascular networks. *PLoS Comput. Biol.* **13**, e1005392 (2017).
61. K. J. Kim, J. A. Filosa, Advanced in vitro approach to study neurovascular coupling mechanisms in the brain microcirculation. *J. Physiol.* **590**, 1757–1770 (2012).
62. K. J. Kim *et al.*, Astrocyte contributions to flow/pressure-evoked parenchymal arteriole vasoconstriction. *J. Neurosci.* **35**, 8245–8257 (2015).
63. K. J. Kim *et al.*, Vasculo-neuronal coupling: Retrograde vascular communication to brain neurons. *J. Neurosci.* **36**, 12624–12639 (2016).
64. A. Wirth *et al.*, G12–G13-LARG-mediated signaling in vascular smooth muscle is required for salt-induced hypertension. *Nat. Med.* **14**, 64–68 (2008).